

# Microbial Activities' Influence on Three Kinds of Metal Material Corrosion Behaviors

Xia Li, Haiyan Chen, Pimao Chen, Chuangxing Qing, and Huanyuan Li

(Submitted February 16, 2016; in revised form March 12, 2017; published online April 11, 2017)

The corrosion behaviors of copper, 6063 aluminum alloy, and Q235 steel were investigated by open-circuit potential (OCP), anodic polarization curve analysis, and electrochemical impedance spectroscopy (EIS). Scanning electron microscopy revealed that a small number of translucent rod-shaped bacterial colonies on the copper surface of copper, whereas plenty of rod-shaped microbes colony were detected on the surface of 6063 aluminum material. Moreover, rod-shaped bacteria and mold colonies attached to the surface of Q235 steel. The decrease in the OCP of copper, 6063 aluminum alloy, and Q235 steel led to higher corrosion tendency. EIS analysis showed that bacteria can reduce the value of AC impedance of copper, the polarization resistance, and the surface resistance, thereby accelerating corrosion. Moreover, the polarization resistance of aluminum alloy in bacterial seawater is lower than that in non-bacterial seawater, indicating the existence of bacteria accelerated the corrosion of 6063 aluminum alloy. The adherence of microbes on Q235 steel surface accelerated the dissolution of the surface layer, and then the passive film is replaced by incompact biofilm layer. Q235 steel corrodes faster under the influence of bacteria because the polarization resistance in bacterial seawater is much lower than that in non-bacterial seawater.

**Keywords** aluminum alloy, copper, electrochemical impedance spectroscopy, microbiologically influenced corrosion, salinity, seawater, steel

## 1. Introduction

Oceans cover approximately 70 percent of the Earth's surface and are a significant natural resource. The growing demand of scientific explorations and developments in the deep sea requires a large amount of corrosion-resistant metallic structures, because seawater contains large amounts of chloridion, halo-bios, and macro-dwellers, which are highly corrosive. The biofilm sticking to the surface of metallic materials causes the corrosion of metallic structures. Statistics shows that the attachment of bacteria and the growth of biofilms account for approximately 70-80% of effective material loss, which leads to the loss of 7-10 billion dollars each year (Ref 1). Microbiologically influenced corrosion (MIC) of seawater conditions is a long-term problem of human beings.

Although researchers have made progress in the MIC corrosion mechanism, the study on the MIC reaction is still in the primary stage due to the complexity of the MIC system, the

chemical reaction, the electrochemical reaction, and the biochemical reaction in the process of corrosion. Castaneda et al. (Ref 2) found that the non-uniform adsorption of sulfate-reducing bacteria (SRB)-biofilm under the artificial seawater conditions could expand the active site of the corrosion region through the study of the electrochemical effects of SRB on the interface of Q235 carbon steel. In the study of the electrochemical behavior and corrosion mechanism of carbon steel, Javaherdashti et al. (Ref 3) found that the failure time of carbon steel immersed in iron-reducing bacterial (IRB) medium was shorter compared with that in the sterile medium. This result indicated that IRB could accelerate corrosion. Yu et al. (Ref 4) studied the corrosion behavior of Q235 carbon steel under SRB electroactive biofilm by electrochemical impedance spectroscopy (EIS) technique. The SRB biofilm could directly obtain the accelerated corrosion rate of carbon steel from the metal surface. Adbullah et al. (Ref 5) used polarimetric curves to study the corrosion behavior of API 5L X-70 carbon steel in SRB environment. The corrosion rate of carbon steel calculated by Tafel slope was similar to that of weight loss method. In seawater, the effect of microorganisms on the corrosion of metallic materials is more complex and severe. Studies on the MIC for aluminum, copper, and alloy materials (Ref 2-12) are rarely reported compared with that of carbon steel. Most of these studies have focused on typical carbon steel corrosion mechanism caused by ocean microbial communities, and no research is focused on other metallic materials.

In the preset study, microorganisms were cultivated in seawater under laboratory condition. The corrosion behaviors and mechanism of carbon steel, aluminum alloy, and copper caused by microorganisms are studied by the measurement of open-circuit potential (OCP), polarization curves, and EIS. The investigation of the mechanism of MIC conducive contributes to the study on not only the reaction between the surfaces of metallic materials and microbes but also the MIC process. Enhancing the corrosion-resistant properties of metallic materials under seawater with microbes is important. In this study,

**Xia Li**, Faculty of Environmental and Biological Engineering, Guangdong University of Petrochemical Technology, No. 139 Guandu 2nd Street, Maoming 525000, Guangdong, People's Republic of China; **Haiyan Chen** and **Huanyuan Li**, School of Materials and Energy, Guangdong University of Technology, Guangzhou 510006, Guangdong, People's Republic of China; and **Pimao Chen** and **Chuangxing Qing**, South China Sea Fisheries Research Institute, Chinese Academy of Fishery Science, Guangzhou 510300, Guangdong, People's Republic of China. Contact e-mail: mmlxia2006@163.com.

we provide a scientific basis for establishing a reasonable and valid procedure for the systematic control of MIC.

## 2. Materials and Methods

### 2.1 Materials

Copper T2 (Bi 0.001, Sb 0.002, As 0.002, Fe 0.005, Pb 0.005, S 0.005, Cu margin), 6063 aluminum alloy (Si 0.20-0.6, Cu  $\leq$  0.10, Mg 0.45-0.9, Zn  $\leq$  0.10, Mn  $\leq$  0.10, Ti  $\leq$  0.10, Cr  $\leq$  0.10, Fe 0.000-0.350, Al resid), Q235 carbon steel, and seawater (obtained from Daya Bay, Huizhou, Guangdong, China; salinity is 30.26, oxygen content is 5.96 mg/L, and pH is 7.25) were used in this study.

### 2.2 Methods

**2.2.1 Sample Preparation.** The metal samples for electrochemical measurement were cut into small sheets of 10 mm  $\times$  10 mm. Then, the untested surfaces were connected to wires by soldering, and the samples were sealed by waterproof glue.

Before the experiments, the metallic surfaces were rubbed with fine sandpapers (above 800 meshes) sealed by glue stick, degreased, washed, dried, and fixed wire by soldering on the no-test surfaces. Samples for corrosion rate measuring were cut into small sheets of 55 mm  $\times$  55 mm and rubbed, washed, and dried before further use.

**2.2.2 Culturing of Bacteria.** The growth medium was composed of tryptone 10 g/L, peptone 5 g/L, and yeast extract powder 1 g/L. NaOH solution was used to adjust pH to the range of  $7.0 \pm 0.2$ , which is the typical culture media pH designed for marine microbes. The compounded culture media were poured into Erlenmeyer flasks, which were covered with gauze on the top. The Erlenmeyer flasks were sterilized at 120 °C. The bacterial seawater was prepared by mixing the non-sterilized seawater with the culture media at the volume proportion of 1:10, while the non-bacterial seawater is prepared by mixing the sterilized seawater with the culture media at the volume proportion of 1:10. The cultured bacteria were nurtured in an oven-controlled crystal oscillator. The absorbency of both samples was measured every 4 h by a spectrophotometer to plot the bacterial growth curve. The operation glassware used for microbiological analysis was sterilized under high engine temperature and pressure conditions. The seawater was sterilized at 120 °C for 15-30 min, and all experiments were conducted in the ultra-clean workbench. The sterilized seawater samples were stored at temperatures between 25 and 28 °C without light for three days. Then, a spectrophotometer was used to determine the light absorption of the sterilized seawater and to check whether the samples were completely sterilized.

**2.2.3 Morphology of Adhesion Microbes.** The samples were rubbed and polished. Then, they were degreased by acetone and were disinfected by 75% alcohol. Ultraviolet light was used for sterilization, and the samples were immersed into bacterial seawater. When the number of bacteria reached the peak, the biofilm was fixed firmly with glutaraldehyde on the surface. After drying, the morphology and distribution of adhesion microbes on the surface of the samples were observed under a scanning electron microscope (SEM) (AMRAY-100B).

The species of bacteria were determined by matching the types of culture media, growth characteristics, and microbial

morphologies between this study and the authoritative microbe manual. The bacteria-containing liquid samples were dropped on the sterilized silicon wafers by pipettes then observed under SEM.

**2.2.4 Electrochemical Testing.** The corrosive media were split into two groups for electrochemical measurement: One was bacterial seawater which was kept in an oven-controlled crystal oscillator for 30 h; the other one was non-bacterial seawater containing culture medium, which was sterilized by ultraviolet light serving. (1) OCP: A UJ25 direct-current high-potential-difference meter was used to measure the OCP using saturated calomel electrode as reference electrode. The electric potential was measured, and the saturated calomel electrode potential was used as reference. (2) Anodic polarization curve and electrochemical impedance: to investigate the corrosion behaviors of materials in different corrosion environments, an electrochemical IM6 workstation made in Germany was used to measure the anodic polarization curve by steady-state potentiostatic method; a saturated calomel electrode and a platinum electrode were used as a reference electrode and an auxiliary electrode, respectively, with a scanning rate of 40 mV/min. EIS was performed using an automat electrochemical workstation in the range of frequencies between  $1 \times 10^{-2}$  and  $1 \times 10^5$  Hz. The perturbation amplitude was set to 5 mV, and the testing temperature was 25 °C.

**2.2.5 Corrosion Rate Measurement.** The samples were exposed to corrosive environments at room temperature for 100 days. To remove the corrosion products on the sample surfaces, the samples were defiled with 15% hydrochloric acid for 3-5 min and brushed with eraser and scrub. The samples were dried and weighed. The bacteria on the samples were batch cultured: the sterilized metal samples were immediately immersed in bacterial seawater in oxygen-rich environment at a temperature of 25 °C for 30 h. After immersion, the samples were fetched out and revaccinated in the culture refreshed media. A spectrophotometer was used to monitor the bacterial growth. The bacteria multiplied every 30 h and were cultured in this manner for 80 cycles.

## 3. Experimental Results and Analysis

### 3.1 Growth Law of Bacteria and the Morphology of Adhesion Microbes

The growth of bacteria is divided into four stages: lag phase, exponential growth phase, plateau phase, and decline phase. Figure 1 shows the growth curve of bacteria from Daya Bay seawater. At the initial 8 h, the bacteria were in the lag phase. In the subsequent 8 h, the population of the bacteria dramatically increased in the exponential growth phase. In the next 14 h, bacterial multiplication leads to a balance between the birth and the death rate. The population of bacteria reached a peak after 30 h. After 35 h, the lack of nutrients in culture media caused more deaths than births, which resulted in sharp decline in the bacterial number. This stage is called the decline phase.

After the samples were immersed into the bacterial seawater for 30 h, the morphologies of adhesion microbes are shown in Fig. 2. Though a single layer containing toxic solution was formed on the surface of copper, which provides copper an

ability to prevent bio-fouling, a small amount of rod-shaped translucent bacteria were still observed on the surface of copper (See Fig. 2a). Figure 2(b) illustrates that the surface of the 6063 aluminum was covered with dense rod-shaped microorganisms and the variations of their size, length, camber, and thickness were small. Most bacteria are 2-3  $\mu\text{m}$  long and 0.3-1  $\mu\text{m}$  wide. The structure of adhering microbes of Q235 steel is shown in Fig. 2(c) and (d). Visible cracks existed on the surface of the biofilm of Q235 steel samples, because the increasing thickness of the biofilms leads to the increase in the stress. Figure 2(c) shows that the molds colony was attached to the surface of Q235, and the basic unit of mold bacteria was the hyphen, which presents a tubular shape with 2-10  $\mu\text{m}$  long. The bacteria can constantly grow forward and bifurcate (Ref 13). Besides molds, *Bacillus* colonies were found on the surface of Q235, as shown in Fig. 2(d).

### 3.2 Open-Circuit Potentials

The three kinds of metal samples were immersed in the seawater media with bacteria and non-bacterial seawater media.

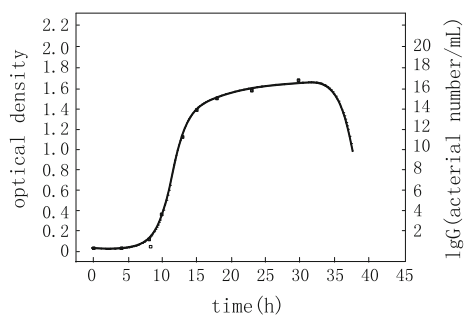


Fig. 1 Growth curves of the bacteria

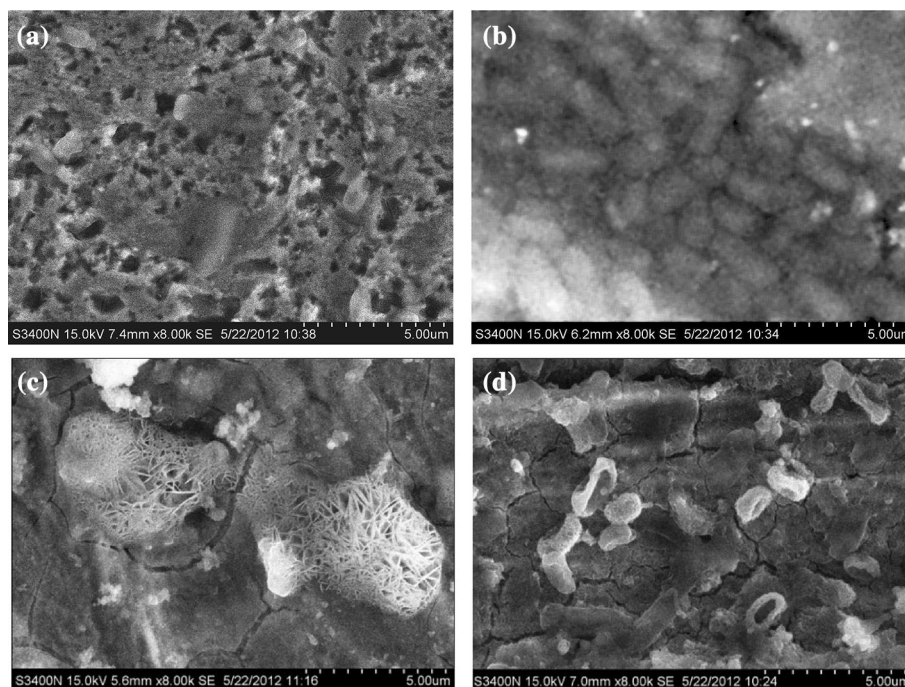


Fig. 2 SEM of the microbe adhesions (a) copper; (b) 6063 aluminum alloy; (c) Q235 steel; (d) Q235steel

The changes of OCP over time are shown in Fig. 3. The corrosion self-electric potential of the three kinds of material electrodes went down over time, and neither in bacterial seawater or non-bacterial seawater, forming dense passive films through copper, aluminum alloy, and Q235 steel in chloridion-rich seawater is impossible. The OCP of copper in non-bacterial seawater was the largest and that in bacterial seawater was the second largest among the samples in six different media, which indicates that copper has the highest thermodynamic stability in the three kinds of metals. The corrosion tendency of copper increased due to the adherence of rod-shaped bacteria on the surface of copper samples and the possibility to produce some special chemicals during their complicated living activity, such as metabolism. Comparing curves 3 and 4, the existence of bacteria significantly deduced the OCPs and increased the corrosion tendency of aluminum alloy. The comparison between curves 5 and 6 showed that the OCPs of Q235 steel becomes more negative due to the existence of rod-shaped bacteria and mold.

### 3.3 Anodic Polarization Curve

The three kinds of metal electrodes immersed in bacterial medium and non-bacterial medium anodic polarization are shown in Fig. 4. Curves 1 and 2 in Fig. 4 are the anodic polarization curves of copper in bacterial seawater and non-bacterial seawater. The active area, active-passivation transition area, passivation area, and transpassive area all exist in both curves. As shown in Fig. 4, curve 1 has lower OCP and greater maintaining passivity current density than those of curve 2, which indicates that the existence of microorganisms facilitates the corrosion of copper.

Curves 3 and 4 are the anodic polarization curves of aluminum alloy electrodes in bacterial media and non-bacterial media. None of the active-passive transition region is found in the polarization curves of aluminum alloy. During the passi-

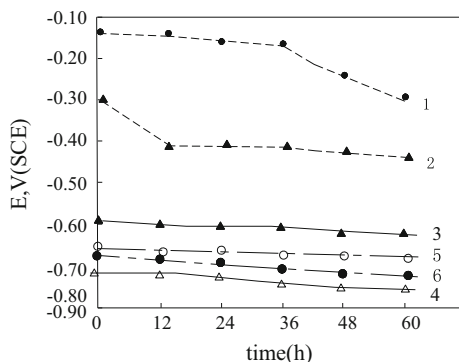


**Fig. 3** Open-circuit potential curves (1) copper in non-bacterial seawater; (2) copper in bacterial seawater; (3) 6063 aluminum alloy in non-bacterial seawater; (4) 6063 aluminum alloy in bacterial seawater; (5) Q235 in non-bacterial seawater; (6) Q235 steel in bacterial seawater

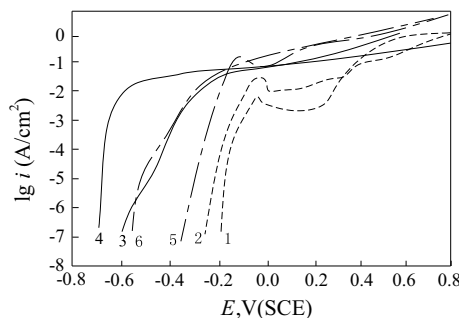


**Fig. 4** Anode polarization curve (1) copper in non-bacterial seawater; (2) copper in bacterial seawater; (3) 6063 aluminum alloy in non-bacterial seawater; (4) 6063 aluminum alloy in bacterial seawater; (5) Q235 in non-bacterial seawater; (6) Q235 steel in bacterial seawater

vation, the corrosion current accelerates and remains a constant value with increasing potential, maintaining passivity current density at approximately  $5.82 \times 10^{-2} \text{ A/cm}^2$ . This result indicates that though the passive film is formed on the surface of aluminum alloy, the selective penetration of chloride ion allows the passive film of aluminum alloy to possess a fast dissolving rate due to the porosity and discreteness of the passive film structure. The self-corrosion electric potential of 6063 aluminum alloy in bacterial seawater is  $-0.73 \text{ V}$ , which is lower than that in non-bacterial seawater ( $-0.52 \text{ V}$ ). These results indicate that the adherence and reproduction of microbes reduce the corrosion resistance of aluminum alloy. The major factor affecting the anticorrosion is that bacteria significantly deduce the self-corrosion electric potential of aluminum alloy. The existence of bacteria reduces the system's thermodynamic stability.

Curves 5 and 6 are the anodic polarization curves of Q235 steel in non-bacterial and bacterial media. In the non-bacterial environment, the anodic polarization curves possess narrow active-passivation transition area, besides it possesses a wider transpassive area; these indicate that the film on the Q235 steel is unstable. In the bacterial environment, the curve immediately jumps into the transpassive area from the active area and shows that the formation of passive film of Q235 was restrained under the microbial effect. The self-corrosion electric potential is

more negative under the condition of bacterial environment due to the changes of the composition among the oxygen content, ammonia content, and pH with the growth and metabolism of bacteria. The more negative self-corrosion potential causes the decline of the thermodynamic stability of steel. As shown in Fig. 4, the natural corrosion potential is within 0.01 V. The current density of curve 4 is larger than that of curve 3, which indicates that bacteria facilitates the corrosion of aluminum alloy before the breakdown of the passive film. In the passivation area (the corrosion potential is greater than 0.01 V), however, the aluminum alloy was protected by the bacterial film.

### 3.4 Corrosion Rate

The three kinds of metal samples were exposed into bacterial seawater media and non-bacterial seawater media in different salinities for 100 days. The results are shown below in Table 1.

As shown in Table 1, copper has the lowest corrosion rate among the three kinds of materials. Although the number of attached microbes is small, the copper is still sensitive to MIC and the corrosion is aggravated by bacteria. In Fig. 5, XRD data show that the products were mainly  $\text{CuCl}$  and  $\text{Cu(OH)Cl}$  after the corrosion of copper. The corrosion rate of 6063 aluminum alloy in non-bacterial seawater is  $0.148 \text{ mm/a}$ , which is higher than that of copper in the same medium. As shown in Fig. 6, the main product was  $\text{Al}_2\text{O}_3$  after the corrosion on the surface for 6063 aluminum. The OCP of aluminum alloy is more negative than that of copper, because high concentrations of chloride ion around the surface accelerates the dissolving of passive film. That is, 6063 aluminum alloy has poorer corrosion resistance than copper in both thermodynamic and kinetic perspectives. In the presence of bacteria, a large amount of bacterial colonies cover the surface of aluminum alloy. As the reaction proceeds, the metabolism of microbes and the accumulation of metabolites below the biofilm have changed the interface conditions, such as pH, dissolved oxygen, ammonia content, and the surface roughness between the aluminum alloy and the media. These conditions significantly reduce the OCP of aluminum alloy (as shown in Fig. 3 and 4) and significantly minimized the electrochemical corrosion of thermodynamic stability resulting in the acceleration of aluminum alloy corrosion. The corrosion rate of Q235 in non-bacterial seawater is relatively high ( $0.285 \text{ mm/a}$ ). It is usually attributed to the high tendency of oxygen reduction when oxygen, chloride ion, and water are sufficient. In Fig. 7, XRD analysis shows that the major chemicals of corrosion products which attached to the surface of steel are  $\text{Fe(OH)}_3$ ,  $\text{Fe(OH)}_2$ ,  $\text{FeO}$ ,  $\text{FeOOH}$ ,  $\text{Fe}_3\text{O}_4$ , and  $\text{Fe}_2\text{O}_3$ . Their porous structure contributed to the prevention of further corrosion. Combined with the effect of both high chloride ion concentration and ocean microbes, the thermodynamic stability of steel largely reduces. That explains the highest corrosion rate of  $0.409 \text{ mm/a}$  among the materials in the experiments.

### 3.5 Electrochemical Impedance Spectroscopy

To demonstrate the electrochemical mechanism of the MIC in metal (Ref 14, 15), an automat electrochemical workstation was used to measure the EIS of the samples. The electrochemical impedance diagrams of each sample immersed in non-bacterial and bacterial seawater for 30 h are shown in Fig. 8. The Bode diagrams of the three kinds of metal samples are

**Table 1 Corrosion rate of 3 kinds of metals**

Material Seawater	Pure copper		6063 Aluminum alloy		Q235 steel	
	Without bacteria	With bacteria	Without bacteria	With bacteria	Without bacteria	With bacteria
Corrosion rate (mm/a)	0.037	0.121	0.148	0.353	0.285	0.409

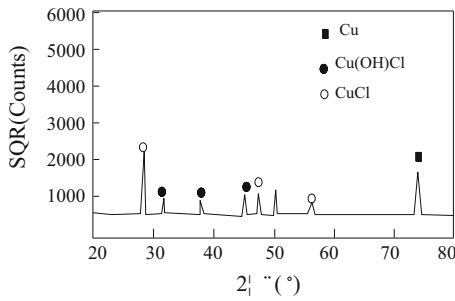


**Fig. 5** XRD spectrums of copper

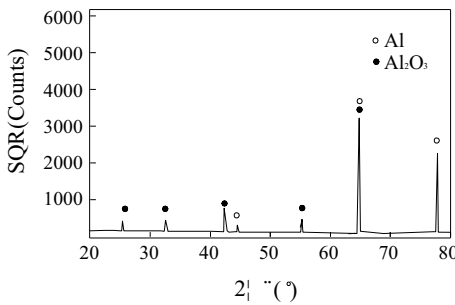


**Fig. 6** XRD spectrums of 6063 aluminum

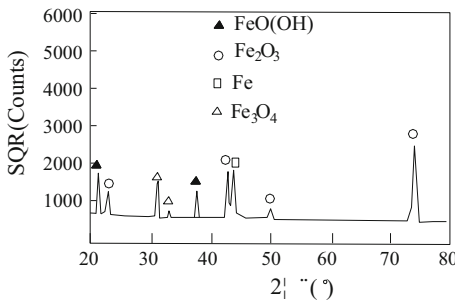


**Fig. 7** XRD spectrums of Q235 steel

shown in the curves of *phase-f* on Fig. 8(b), (e), and (f). The three kinds of metal samples show four peaks, which indicate that copper, aluminum alloy, and steel possess four characteristic frequencies. That is, their curve possesses time constants. Solution resistance ( $R_s$ ) was treated as the  $R(Q(R(RM)))$  in the composite equivalent circuit in seawater, where  $R$  is the equivalent resistance and  $Q$  is the constant phase angle element. The electric double layer of the interface between electrode and solution is generally treated as a capacitor in the circuit. However, the frequency response characteristics of electric double layer capacitance between solid electrodes are not the same as that of the pure capacitance. In the electric double layer containing solid electrodes, the dispersive effect has to be considered and is regarded as the equivalent element ( $Q$ ). The expression of element  $Q$  is:

$$Y_Q = Y_0 \omega^n \cos\left(\frac{n\pi}{2}\right) + jY_0 \omega^n \sin\left(\frac{n\pi}{2}\right),$$

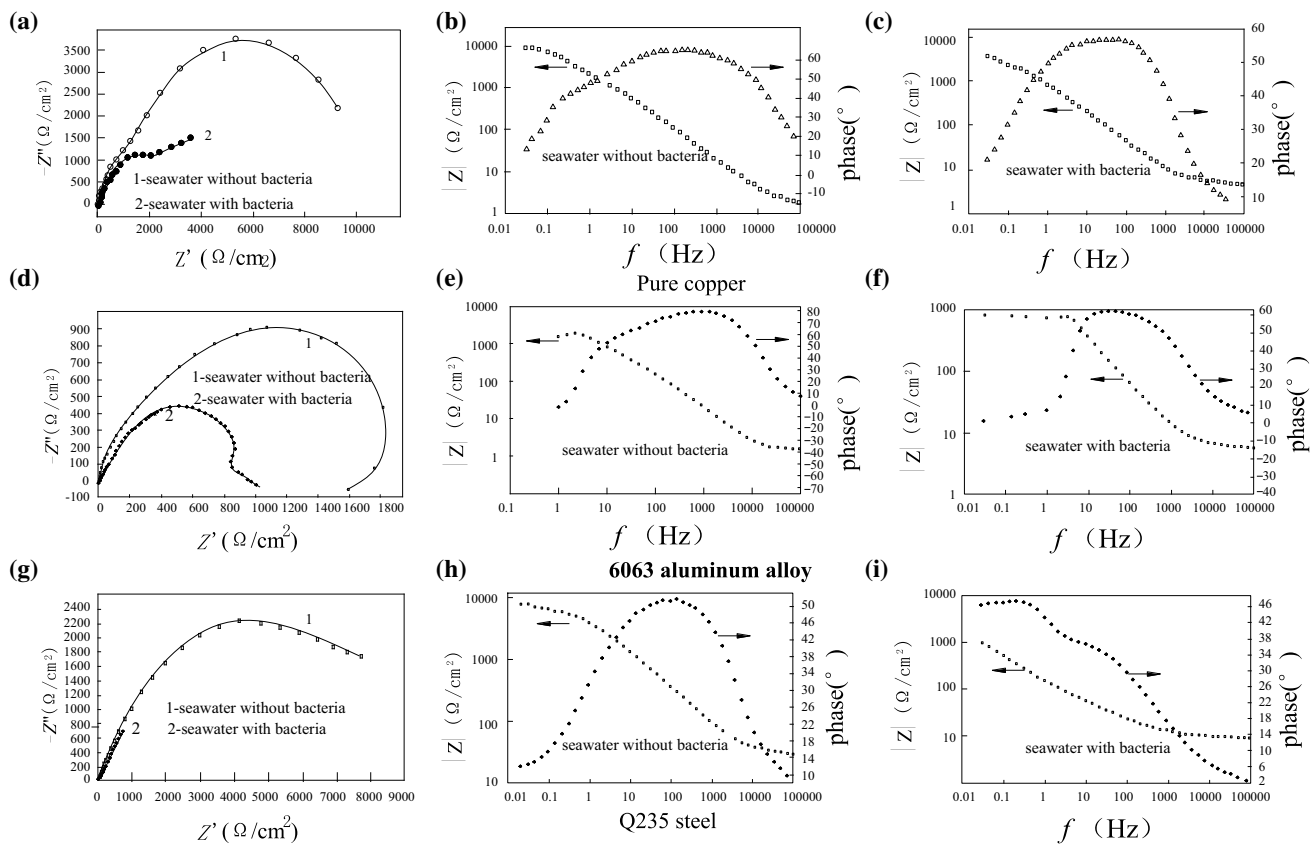
where  $n$  is in the range between 0 and 1, and  $\omega$  is the high frequency state variables. If  $n = 0(n = 1)$ ,  $Q$  equals  $R(C)$ . Based on the high frequency characteristics in the EIS figures of various metallic materials,  $\omega$  can be tuned. The equivalent circuit diagram in Fig. 9 is generated by fitting the impedance spectrum of each system using ZSIMPWIN software. From the Nyquist plots of impedance of the three kinds of materials in Fig. 8, the arc radius representing the magnitude of electrochemical capacitance in bacterial seawater was larger than that in non-bacterial seawater.

Figure 8(a)-(c) show the electrochemical impedance diagrams of copper immersed in non-bacterial and bacterial seawater for 30 h. As shown in Fig. 8(a), copper in bacterial seawater has smaller electrochemical capacitance radius than that in non-bacterial seawater, which indicates that the existence of bacteria reduces the impedance magnitude of copper in seawater. The diagram of copper in bacterial seawater illustrates that the feature of typical Warburg impedance in the low-frequency band, such as a line of  $45^\circ$  inclination at the low-frequency region, which indicates that both electrochemical polarization and concentration polarization control the corrosion behavior of copper in bacterial seawater. Therefore,  $M = (RW)$ , copper was treated as an equivalent circuit in the form of  $R_s(Q(R_t(Q_p(R_pW))))$ . As shown in Fig. 9(a), fitting process was conducted to obtain the optimal equivalent circuit on all test dates of electrochemical impedance spectroscopy by using ZSIMPWIN. The optimal equivalent circuit of copper in bacterial seawater is shown in Fig. 9(b). Formulas (1) and (2) are the expressions of Faradaic admittance deduced from the equivalent circuits shown in Fig. 9(a) and (b):

$$Z_a = R_s + \frac{1}{Y_Q + \frac{1}{R_t} + \frac{1}{j\omega C_p + \frac{1}{R_p}}} \quad (\text{Eq 1})$$

$$Z_b = R_s + \frac{1}{Y_Q + \frac{1}{R_t} + \frac{1}{j\omega C_p + \frac{1}{R_p + Z_w}}} \quad (\text{Eq 2})$$

In the formulas,  $R_s$  is the solution resistance from the orifice of a Luggin capillary against reference electrode to working electrode,  $Y_Q$  is the admittance of the resistor element of copper surface film layer,  $R_t$  is the resistance of copper surface film layer,  $j\omega C_p$  is the electric double layer admittance,  $R_p$  is the polarization resistance, and  $Z_w$  is the Faradaic admittance caused by diffusion process.  $Y_Q$  can be written in the following expression:  $Y_Q = Y_0 \omega^n \cos\left(\frac{n\pi}{2}\right) + jY_0 \omega^n \sin\left(\frac{n\pi}{2}\right)$ . The fitted values of all effective circuit parameters are shown in Table 2. In the non-bacterial environment, the resistance of copper surface film layer ( $R_t$ ) was high ( $6188 \Omega/\text{cm}^2$ ) and shows that a relatively complete barrier films has formed on the surface of sample to protect the substrate from corrosion. Meanwhile, polarization resistance ( $R_p$ ) was relatively high ( $6188 \Omega/\text{cm}^2$ ),



**Fig. 8** EIS diagrams of copper after 30 h of immersion in different mediums (a) nyquist diagram of pure copper in seawater; (b) bode diagram of pure copper in seawater without bacteria; (c) bode diagram of pure copper in seawater with bacteria; (d) nyquist diagram of 6063 aluminum alloy in seawater; (e) bode diagram of 6063 aluminum alloy in seawater without bacteria; (f) bode diagram of 6063 aluminum alloy in seawater with bacteria; (g) nyquist diagram of Q235 steel in seawater; (h) bode diagram of Q235 steel in seawater without bacteria; (i) bode diagram of Q235 steel in seawater with bacteria

which shows that the dissolving of copper exhibited severe retardation during the corrosion process as shown in Table 2.

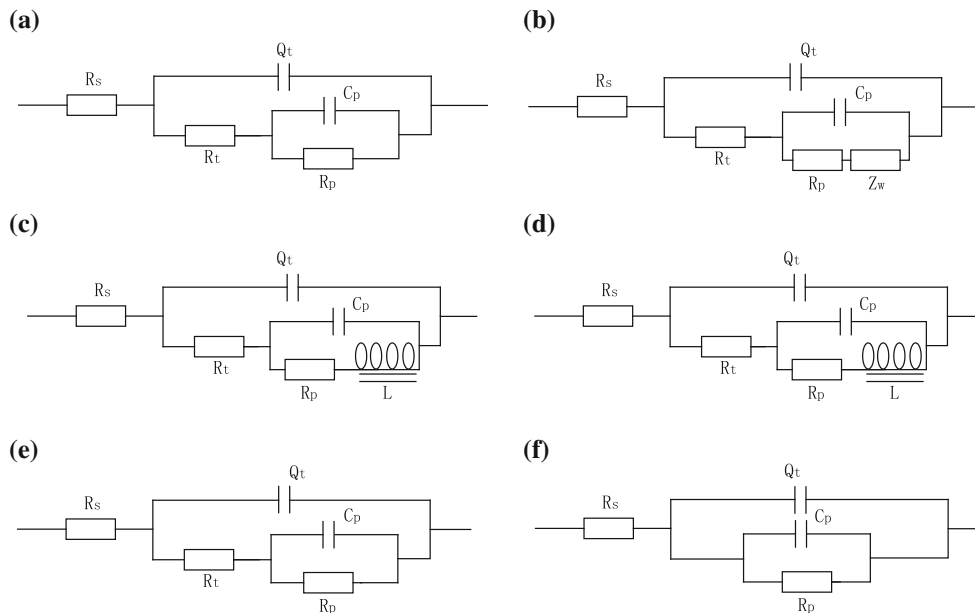
When bacteria are accumulated in the seawater, the living activities of bacteria lead to the dissolution and the formation of cracks on the surface of the film. These activities caused the formation of local defects on the film's surface and the increase of porosity and roughness resulting in the resistance reduction of the copper's surface film layer ( $R_t$ ). Meanwhile, the polarization resistance ( $R_p$ ) decreases responding to the effect of bacteria, which accelerated the corrosion rate. The value of the resistor element about the oxide layer on the surface indicates that copper surface has many small pits because of the adherence of loose and heterogeneous biofilm, which contributes to the increase in the specific surface area. Therefore, bacterial activity increases the permittivity ( $Q_t$ ) on the copper surface. The polarization of biofilm is due to the difference in the concentrations of reactants in the interfacial region and the bulk of solution. Thus, compared to the electrochemical reaction, the diffusion of the Warburg impedance dominates in the low-frequency band.

Figure 8(d) shows the electrochemical impedance diagram of aluminum alloy immersed in non-bacterial and bacterial seawater for 30 h. Different from copper and steel, the aluminum alloy curve in the high frequency region is in the IV Quadrant in its Nyquist diagram, indicating that inductance ( $M = RL$ ) was detected during the corrosion process. Therefore, aluminum alloy was defined as an equivalent circuit in the form of  $R_s(Q_t(R_t(C_p(R_pL))))$ . The low-frequency inductance loop

emerged on the EIS implies that the aluminum alloy is in the pit incubation period. In this period, the chloride ion leads to the dissolution of passive film of aluminum alloy. Thus, the surface resistance of passive film in the  $Cl^-$  absorption region is much lower than that in the low- $Cl^-$  concentration region. In the  $Cl^-$  absorption region, the low surface resistance increases the current density near the surface area. Meanwhile, aluminum ion enters into the solution at a rather high speed. The hydrolyzation of aluminum ions leads to the increase in the  $H^+$  concentration near the metal's surface. Simultaneously, the electromigration caused by the high anodic current density increases the concentration of chloride ions in the solution layer contacting with metal surface area. The increasing concentration of  $H^+$  and  $Cl^-$  accelerates the dissolution of the passive film on the surface area, which is called "autocatalytic effect". Thus, this effect constantly decreases the thickness of the passive film in these surface areas. Fitting process was conducted to obtain the optimal equivalent circuit on all test dates of electrochemical impedance spectroscopy by ZSIMP-WIN to obtain the optimal equivalent circuit as shown in Fig. 9(c) and (d). The expressions of Faradaic admittance deduced from the equivalent circuits were expressed as follows:

$$Z_c = R_s + \frac{1}{Y_Q + \frac{1}{R_t} + \frac{1}{Y_{C_p} + \frac{1}{R_p + j\omega L}}} \quad (\text{Eq 3})$$

In the formula,  $R_s$  is the solution resistance from the orifice of a Luggin capillary against reference electrode to working



**Fig. 9** Equivalent circuit models for electrodes in different mediums (a) Pure copper in seawater without bacteria; (b) Pure copper in seawater with bacteria; (c) 6063 aluminum alloy in seawater without bacteria; (d) 6063 aluminum alloy in seawater with bacteria; (e) Q235 steel in seawater without bacteria; (f) Q235 steel in seawater with bacteria. [Rs is the solution resistance from the orifice of a Luggin Capillary against reference electrode to working electrode; Rt is the resistor element of metal surface film layer; Qt is the constant phase angle element of metal surface film layer; Ct is the capacity of metal surface film layer; Rp is the polarization resistance; Cp is the electric double layer capacitor; Qp is the electric double layer constant phase angle element; Zw is the faradaic impedance caused by diffusion process; L is the equivalent inductance]

**Table 2** Parameter values of elements in the equivalent circuit models

Material	Mediums	$R_s, \Omega/\text{cm}^2$	$R_t, \Omega/\text{cm}^2$	$R_p, \Omega/\text{cm}^2$	$Q_t, \text{s}^n/\text{cm}^2$	$C_p, \text{F}/\text{cm}^2$	$L, \text{H}/\text{cm}^2$	Warburg, $\text{S}^5/\text{cm}^2$
Pure copper	Without bacteria	1.658	4412.000	6188.000	$Y_0 = 7.257 \times 10^{-5}, n = 0.7493$	$9.918 \times 10^{-5}$	...	...
	With bacteria	4.404	7.125	4615.000	$Y_0 = 3.345 \times 10^{-4}, n = 0.6368$	$5.361 \times 10^{-6}$	...	0.01353
6063 aluminum alloy	Without bacteria	1.330	0.447	1743	$Y_0 = 1.469 \times 10^{-4}, n = 0.447$	$7.120 \times 10^{-6}$	210.5	...
	With bacteria	5.562	0.480	802	$Y_0 = 1.675 \times 10^{-4}, n = 0.6975$	$2.569 \times 10^{-6}$	43.33	...
Q235 steel	Without bacteria	25.93	36.833	8213	$Y_0 = 5.173 \times 10^{-5}, n = 0.6057$	$3.16 \times 10^{-7}$	...	...
	With bacteria	8.749	...	682.2	$Y_0 = 2.27 \times 10^{-3}, n = 0.800$	$2.159 \times 10^{-4}$	...	...

electrode,  $Y_Q$  is the admittance of the resistor element of copper surface film layer,  $R_t$  is the resistance of copper surface film layer,  $j\omega C_p$  is the electric double layer admittance,  $R_p$  is the polarization resistance, and  $j\omega L$  is the resistance of equivalent inductance. The fitted value of all equivalent circuit parameters is shown in Table 2. As listed in Table 2, the surface film layer's resistance of 6063 aluminum alloy in both bacterial and non-bacterial seawater ( $R_t$ ) is low ( $<0.5 \Omega/\text{cm}^2$ ) and shows that the chloride ion attached to the surface of aluminum alloy's passive film is uniformly in the seawater, which accelerates the film's dissolution. The resistance value is relatively low in the surface area with the adherence of chloride ions in the seawater. From the phase angle–frequency diagrams in Fig. 8(e) and (f), the phase angle of aluminum alloy in both bacterial and non-bacterial seawater are smaller than  $-45^\circ$ , showing that the current is equally distributed. The corrosion rate can be characterized by the polarization resistance. As shown in Table 2, the polarization resistance ( $R_p$ ) of aluminum alloy in bacterial seawater is  $802 \Omega/\text{cm}^2$  less than that in the non-bacterial seawater ( $1743 \Omega/\text{cm}^2$ ), indicating that the existence of bacteria accelerates the corrosion of 6063 aluminum alloy.

The fitted equivalent circuit of Q235 steel in non-bacterial seawater is plotted in Fig. 9(e). The expression of Faradaic admittance is shown as Formula (1). The data from Table 2 imply that the existence of bacteria accelerates the dissolution of the steel and the formation of the incompact biofilm layer, because the bacteria on the surface of Q235 steel consume oxygen through its vital movement and produce various substances, such as enzymes, sulfides, and ammonia (Ref 16). This phenomenon accelerated the dissolution the steel surface layer, which was replaced with incompact biofilm layer. Many cracks exist on the biofilm surface of steel shown in Fig. 2(c) and (d). Thus, resistance does not exist on the surface of steel in the bacterial environment. As shown in Fig. 8(h) and (i), the phase angle–frequency diagrams in the bode figure show that the phase angles of Q235 steel in both bacterial and non-bacterial seawater are smaller than  $-45^\circ$ . The polarization resistance ( $R_p$ ) is inversely proportional to the corrosion rate in the circuit based on in-line transport. The polarization resistance of Q235 steel in bacterial seawater is one order of magnitude smaller than that in non-bacterial seawater, thus the corrosion rate of Q235 steel was faster under the influence of bacteria.

## 4. Conclusions

1. A small number of translucent rod-shaped bacteria existed on the copper surface, whereas rod-shaped microbe colonies were detected on the surface of 6063 aluminum material. Cracks were found in the biofilm clinging to the surface of the Q235 steel samples, and the films were attached by mold and rod-shaped bacteria. The existence of bacteria reduces the OCP of copper, 6063 aluminum alloy, and Q235 steel and decreases their thermodynamic stability, thereby accelerating corrosion.
2. Bacterial activities cause partial dissolution and cracking of the surface of the copper film, leading to the formation of surface defects and the increase in the surface porosity. The decrease in the resistance of copper's surface film and the polarization resistance ( $R_p$ ) accelerate the corrosion rate. The low-frequency inductance loop can be found on the EIS of 6063 aluminum alloy in chloridion-rich seawater and indicates that the passive film is in the pit incubation period. The polarization resistance ( $R_p$ ) is lower in bacterial seawater than that in non-bacterial seawater, which indicates that bacteria accelerate corrosion. The polarization resistance of Q235 steel in bacterial seawater is one order smaller than that in non-bacterial seawater, and thus the Q235 steel corrodes faster under the influence of bacteria.

## Acknowledgments

The authors wish to thank the partners for funding of the project under the program: Guangdong Province Architecture Project (2013B021100020); research subject of state science and technology support program (2012BAD18B02); scientific research of ocean public welfare program (201005013-4); National Natural Science Foundation (41206119); Open Foundation of Scientific Observing and Experimental Station of South China Sea Fishery Resources and Environment, Ministry of Agriculture (SSCS-201208); Open Foundation of Scientific Observing and Experimental Station of South China Sea Fishery Resources and Environment, Ministry of Agriculture (SSCS-201209).

## References

1. T.-H. Tsai, Y.-F. Wu, and S.-C. Yen, A Study of Copper Chemical Mechanical Polishing in Urea-Hydrogen Peroxide Slurry by Electrochemical Impedance Spectroscopy, *Appl. Surf. Sci.*, 2003, **214**(1-4), p 120–135
2. H. Castaneda and X.D. Benetton, SRB-Biofilm Influence in Active Corrosion Sites Formed at the Steel-Electrolyte Interface When Exposed to Artificial Seawater Conditions, *Corros. Sci.*, 2008, **50**(4), p 1169–1183
3. R. Javaherdashti, R.K.S. Raman, C. Panter et al., Microbiologically Assisted Stress Corrosion Cracking of Carbon Steel in Mixed and Pure Cultures of Sulfate Reducing Bacteria, *Int. Biodeterior. Biodegradation*, 2006, **58**(1), p 27–35
4. L. Yu, J.Z. Duan, X.Q. Du et al., Accelerated Anaerobic Corrosion of Electroactive Sulfate-Reducing Bacteria by Electrochemical Impedance Spectroscopy and Chronoamperometry, *Electrochem. Commun.*, 2013, **26**, p 101–104
5. A. Abdullah, N. Yahaya, and N.M. Noor, et al. Microbial Corrosion of API 5L X-70 Carbon Steel by ATCC 7757 and Consortium of Sulfate-Reducing Bacteria. *J. Chem.*, 2014, **2014**, p 1–7
6. H.-Z. Wang, J. Chen, J.-Q. Zhou, S.-W. Yao, and W.-G. Zhang. Corrosion Characteristics of Welded Joints of Copper Pipe in Seawater. *Chin. J. Nonferrous Metals.*, 2006, **16**(4), 645–650
7. P. Szakalos, Corrosion of Copper by Water, *Electrochem. Solid-State Lett.*, 2007, **10**(11), p 63–67
8. J. Sandberg, Corrosion-Induced Copper Runoff from Naturally and Pre-Patinated Copper in a Marine Environment, *Corros. Sci.*, 2006, **48**(12), p 4316–4338
9. Y. Duan, S.-M. Li, J. Du, and J.-H. Liu, Corrosion Behavior of Q235 Steel in the Presence of Pseudomonas and Iron Bacteria, *Acta Phys. Chim. Sin.*, 2010, **26**(12), p 3203–3211
10. X. Sheng, Evaluation of an Organic Corrosion Inhibitor on a Biotic Corrosion and Microbiologically Influenced Corrosion of Mild Steel, *Ind. Eng. Chem. Res.*, 2007, **46**(22), p 7117–7125
11. A.K. Lee, M.G. Buehler, and D.K. Newman. Influence of a Dual-Species Bio-Film on the Corrosion of Mild Steel. *Corros. Sci.* 2006, **48**, 165
12. S.J. Yuan and S.O. Pehkonen, Microbiologically Influenced Corrosion of 304 Stainless Steel by Aerobic Pseudomonas NCIMB2021 Bacteria: AFM and XPS Study, *Collids. Surf. B Bionterfaces*, 2007, **59**(1), p 87–99
13. G.J. Abraham, MIC Failure of Cupronickel Condenser Tube in Fresh Water Application, *Eng. Fail. Anal.*, 2009, **16**(3), p 934–943
14. Q.-X. Cao. Material Corrosion & Protection. Metallurgy Industry Publishing House, Beijing, 2001, p 34–59
15. C.-N. Cao and J.-Q. Zhang. An Introduction to Electrochemical Impedance Spectroscopy. Science Publishing House, Beijing, 2002, p 37–84
16. B.B. Iwona, Corrosion of Technical Materials in the Presence of Bio-Films-Current Understanding and State-of-the- Art Methods of Study, *Intern Biodeter Biodegrad*, 2004, **53**, p 177–183